Investigation of Immobilization of Functionalized Magnetic Nanobeads in Rolling Circle Amplified DNA Coils

Teresa Zardán Gómez de la Torre,[†] Mattias Strömberg,[†] Camilla Russell,[‡] Jenny Göransson,[†,‡] Mats Nilsson,[*,‡] Peter Svedlindh,[*,§] and Maria Strømme[*,†]

Division of Nanotechnology and Functional Materials and Division of Solid State Physics, Department of Engineering Sciences, Uppsala University, The Ångström Laboratory, Box 534, SE-751 21 Uppsala, Sweden, and Department of Genetics and Pathology, Uppsala University, Rudbeck Laboratory, SE-751 85 Uppsala, Sweden

Received: November 26, 2009; Revised Manuscript Received: January 11, 2010

Immobilization characteristics for single-stranded oligonucleotide-functionalized magnetic beads with nominal sizes of 40, 80, 130, and 250 nm in rolling circle amplified (RCA) DNA coils is investigated by employing complex magnetization measurements, dynamic light scattering and fluorescence microscopy. It was found that larger beads in a polydisperse bead size distribution more easily immobilize in the RCA DNA coils than do smaller beads. This may be related to a higher oligonucleotide surface coverage for the larger beads. Furthermore, it was concluded that both bead size and oligonucleotide surface coverage determine whether beads immobilize to give isolated coils with beads or larger clusters of beads and coils. A small bead size and a low oligonucleotide surface coverage favor the first kind of immobilization behavior, whereas a large bead size and a high oligonucleotide surface coverage favor the other. The present findings could be used to optimize both size and surface functionalization of beads employed in substrate-free magnetic biosensors.

1. Introduction

Biofunctionalized magnetic beads have been extensively used in different research and technology areas including biomedicine and diagnostics, because of their useful magnetic properties and biocompatibility. Applications range from bioassays and magnetic separation to hyperthermia cancer treatment and drug delivery.[1–7]

Magnetic biosensors are classified as being either substrate-based (magnetic biochip technology) or substrate-free (lab-on-a-bead technology). In the former category, the presence of the target gives binding of probe-functionalized magnetic beads to the sensor surface, which induces a signal change. Micro-Hall devices[8,9] and GMR sensors[10,11] are examples of substrate-based biosensors. Magnetic biosensors belonging to the latter category rely on measuring changes of magnetic bead properties, most commonly the magnetic relaxation time. When the beads are placed in a magnetic field, the bead magnetic moments will line up with the field. When the field is turned off, the magnetic moments randomize over a period of time. The Brownian relaxation bioassay is an example of a substrate-free method, which makes use of the decrease in the bead Brownian relaxation frequency caused by the hydrodynamic size increase upon probe target hybridization reactions on the surface of the beads.[12] This type of magnetic biosensor has been tested in immunoassays.[13]

Recently, we have demonstrated a novel lab-on-a-bead magnetic biosensor principle for DNA target detection, combining padlock probe target recognition and rolling circle amplification (RCA) with the Brownian relaxation biosensor scheme: the volume-amplified magnetic nanobead detection assay (VAM-NDA).[14–16] The assay begins with padlock probe target recognition followed by ligation, where the ends of the padlock probe molecules are joined together.[17,18] Addition of DNA polymerase initiates the RCA[19,20] and the circularized padlock probes are amplified for a certain time (the RCA time), giving an ensemble of macromolecular DNA coils (RCA coils). The RCA coils are detected by addition of single-stranded oligonucleotide-functionalized magnetic beads exhibiting Brownian relaxation behavior, where the oligonucleotide sequence is complementary to a part of the repeating sequence of the RCA coils. Thus, the beads bind to the RCA coils by base-pair hybridization (bead immobilization) and the hydrodynamic size of the beads is thereby strongly increased, now corresponding essentially to the diameter of an RCA coil, which for an RCA time of 1 h is about 1 μm. This causes a strong decrease of the bead Brownian relaxation frequency (f_B) and the magnitude of the imaginary part (m'') of the complex magnetization ($m = m' - im''$) at f_B for non-immobilized beads, the high-frequency peak (HFP) level, decreases. RCA coils with immobilized beads, including isolated RCA coils with beads and/or clusters of RCA coils with beads, respond by a low-frequency relaxation peak (LFP) in the m'' vs frequency spectrum. Quantitative analysis using the VAM-NDA method can be of the turn-off and/or turn-on type where the former is based on the decrease of the HFP level and the latter is based on the increase of the LFP level with increasing RCA coil concentration.

In previous work, it has been observed that beads with a physical diameter of 40 nm allow for both turn-off and turn-on detection while for bead sizes of 130 and 250 nm only turn-off detection is possible.[15] Furthermore, it has been demonstrated that the number of immobilized beads per RCA coil has a tendency to decrease with increasing bead size. These observations suggest that different bead sizes have different immobilization characteristics.[15]

* Corresponding authors. E-mail: mats.nilsson@genpat.uu.se (M.N.); peter.svedlindh@angstrom.uu.se (P.S.); maria.stromme@angstrom.uu.se (M.S.).

† Division of Nanotechnology and Functional Materials, Department of Engineering Sciences.

‡ Department of Genetics and Pathology.

§ Division of Solid State Physics, Department of Engineering Sciences.

10.1021/jp911251k
Published on Web 02/22/2010

TABLE 1: Properties and Immobilization Characteristics of Oligonucleotide-Functionalized Bead Batches and Sequences of Targets, Padlock Probes, and Detection Probes

batch no.	physical mean diam nonfunctionalized beads (nm)	bead concn (pM)	av no. detection probes/bead	no. amine groups/unit area (nm^{-2})	no. oligonucleotides/unit area (nm^{-2})	PDI[a]	clusters of beads and RCA coils obsd	immobilization in coils of larger beads in bead size distrib
1[b]	40	65450	2	0.37	3.97×10^{-4}	0.136	no	yes
2[c]	40	75946	2	0.37	3.97×10^{-4}		no	yes
3[d]	40	62847	8	0.37	1.59×10^{-3}		no	*f*
4[c,e]	40	51080	14	0.37	2.79×10^{-3}		no	yes
5[b]	80	2768	3	0.60	1.49×10^{-4}	0.087	no	yes
6[c]	80	2765	3	0.60	1.49×10^{-4}		no	yes
7[b,c]	130	2249	2	1.13	3.77×10^{-5}	0.098	no	yes
8[b]	130	2051	14	1.13	2.64×10^{-4}	0.060	yes	no
9[c,e]	130	2882	14	1.13	2.64×10^{-4}		no	no
10[d]	130	2160	10	1.13	1.88×10^{-4}		yes	*f*
11[d]	130	2160	16	1.13	3.01×10^{-4}		yes	*f*
12[b]	250	481	186	3.13	9.47×10^{-4}	0.223	yes	yes
13[c,e]	250	675	186	3.13	9.47×10^{-4}		yes	yes

name	sequence
target	5′-CCCTGGGCTCAACCTAGGAATCGCATTTG-3′ (*Vibrio cholerae* sequence)
padlock probe	5′-TAGGTTGAGCCCAGGGACTTCTAGAGTGTACCGACCTCAGTAGCCGT GACTATCGACTTGTTGATGTCATGTGTCGCACCAAATGCGATTCC-3′
detection probe 1	SH-5′-TTTTTTTTTTTTTTTTTTTTTGTTGATGTCATGTGTCGCAC-3′-FITC
detection probe 2	5′-AGAGTGTACCGACCTCAGTA-3′-Cy3

[a] Polydispersity index (PDI) obtained from DLS measurements of oligonucleotide-functionalized beads in absence of the RCA coils (top-extracted samples, see Figure 2 for details). [b] Used for DLS measurements. [c] Used for magnetic measurements. [d] Used for fluorescence microscopy. [e] The batches are presented in earlier work.[15,16] [f] Not analyzed.

The present study, aiming at achieving increased understanding of the VAM-NDA principle from a fundamental point of view, will evaluate the bead immobilization characteristics for 40, 80, 130, and 250 nm magnetic beads using three experimental methodologies: complex magnetization measurements (magnetic characterization), dynamic light scattering (DLS) and fluorescence microscopy.

2. Experimental Section

2.1. Synthesis of Oligonucleotide-Functionalized Beads Using SPDP Coupling Chemistry and Analysis of Oligonucleotide Surface Coverage. The oligonucleotide-functionalization procedure is described elsewhere.[14,15] Four aqueous suspensions of relatively monodisperse amino group functionalized magnetic nanobeads (nanomag-D NH_2) having nominal diameters of 40, 80, 130, and 250 nm, respectively, were supplied by Micromod Partikeltechnologie, Germany. The oligonucleotide surface coverage was analyzed by a fluorescence-based method.[15] Properties of the synthesized batches of oligonucleotide-functionalized beads are given in Table 1.

2.2. Padlock Probe Target Recognition and RCA. The procedures for target recognition and RCA are described in previous work.[14] An RCA time of 1 h was employed. Target and padlock probe sequences are listed in Table 1.

2.3. Sample Characterization by Complex Magnetization Measurements (Magnetic Characterization). A detailed background is given in the Supporting Information as well as in our earlier publications.[14–16,21,22]

A 25 μL volume of a batch of oligonucleotide-functionalized beads was added to 25 μL of a solution with a given concentration of RCA coils (to obtain a final RCA coil concentration ranging from 0 to 300 pM) containing 250 ng of genomic background derived from a blood sample of a human male individual. A 0 pM sample refers to a negative control sample, i.e., with the absence of RCA coils. The mixture was homogenized and 30 μL was extracted for immediate characterization in a superconducting quantum interference device (SQUID) magnetometer (QD MPMS XL, Quantum Design). The characterization began with 30 min of incubation at 70 °C; thereafter the frequency-dependent magnetic moment was measured at 37 °C (frequency range 1000−0.5 Hz, ac excitation field amplitude 2 Oe). Finally, the saturation magnetic moment was determined at 37 °C in order to obtain the complex magnetization (in units of emu per g of solid content) and for calculating the magnetic bead concentration (diamagnetic contribution from sample holder subtracted).

2.4. Sample Characterization by DLS. A detailed background of DLS is given in the Supporting Information.

A 25 μL volume of a batch of oligonucleotide-functionalized beads was added to 25 μL of a solution with a given concentration of RCA coils (to obtain a final RCA coil concentration ranging from 0 to 100 pM) containing 250 ng of genomic background derived from a blood sample of a human male individual. In the experiments when a 80, 130, or a 250 nm bead batch was used, the mixture was homogenized and incubated for 2 h at room temperature in order to let the immobilized beads sediment to the bottom of the Eppendorf tube. A sample based on 40 nm beads was incubated overnight at room temperature due to slower bead sedimentation. After incubation, 3 μL of the solution was extracted from the top of the mixture and homogenized with 997 μL of sterilized and deionized water. Finally, the hydrodynamic size distribution was measured in this sample using a Malvern Zetasizer Nano ZS (Malvern Instruments Nordic AB), equipped with a 633 nm He−Ne laser and operating at an angle of 173° at 25 °C. This procedure was employed to obtain a size distribution that reflects the size distribution of non-immobilized beads, excluding the sedimented immobilized beads. In other cases, 3 μL of the solution was extracted from the bottom of the mixture and homogenized with 997 μL of sterilized and deionized water. The latter procedure was employed to obtain a size distribution of the sample including the sedimented immobilized beads. We

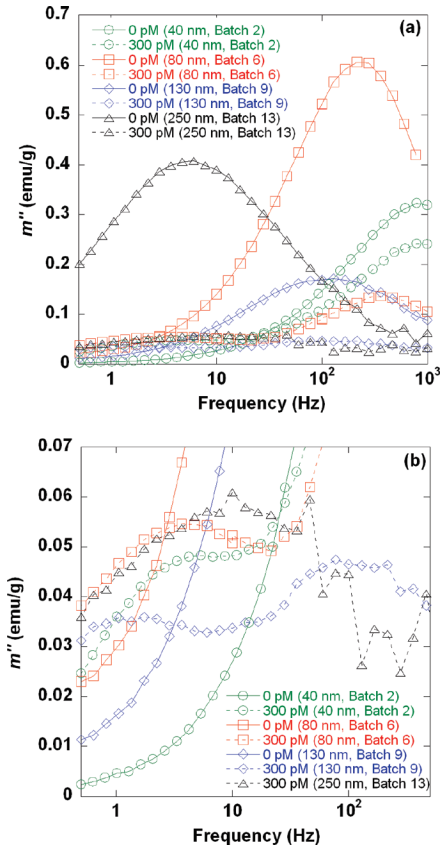

Figure 1. (a) m'' vs frequency spectra at 37 °C for samples with 40 (batch 2), 80 (batch 6), 130 (batch 9), and 250 nm (batch 13) beads and two different RCA coil concentrations (0 and 300 pM). (b) Magnification of the LFPs in panel a. Lines are guides for the eye.

use the notations "top-extracted" and "bottom-extracted" for the two types of samples, respectively. The intensity weighted mean hydrodynamic diameter (*Z*-average) and the polydispersity index (PDI) were calculated by the instrument software. For a detailed definition of these parameters, see the Supporting Information.

2.5. Sample Characterization by Fluorescence Microscopy. RCA coils were produced as previously described[14] and mixed with the beads to obtain a 10 μL solution containing 50 nM Cy3 tagged oligonucleotides (detection probe 2 in Table 1, hybridizing at another position in the RCA coil than the fluorescein isothiocyanate (FITC) labeled oligonucleotide on the beads), 10 pM RCA coils, and 437 nM 40 nm beads (batch 3), 21 nM 130 nm beads (batch 10), or 40 nM 130 nm beads (batch 11). The hybridization was allowed to proceed for 30 min at 55 °C. Poly-L-lysine slides were prepared by cleaning in 0.1% SDS and water and were spun dry. The bead-hybridized RCA coils were thereafter deposited on the slides and dried by incubation for 10 min at 55 °C. The slides were then washed in 1 × PBS and 70% ethanol and spun dry. Vectashield mounting medium was applied and images were registered in an epifluorescence microscope (Axioplan II, Zeiss) equipped with a 100× objective (Fluar, Zeiss) and a 100 W mercury lamp and charge-coupled device camera (C4742-95, Hamamatsu). AxioVision LE 4.3 software (Zeiss) was used for capture of the images.

3. Results and Discussion

3.1. Magnetic Measurements of Bead Immobilization. Figure 1a shows m'' vs frequency spectra at 37 °C for samples with 0 and 300 pM RCA coil concentration and with different bead sizes: 40 (batch 2), 80 (batch 6), 130 (batch 9), and 250 nm (batch 13). Figure 1b provides a magnification of the low-frequency part (0.5−500 Hz) of the spectra in panel a. Note that the low-frequency spectrum recorded for the 250 nm bead negative control sample, which can be studied in detail in panel a, falls outside the plot window in panel b. In panel a, it can be observed that the HFP level for the negative control sample differs depending on bead size. For instance, the 80 nm bead negative control sample shows a larger HFP level than the 40 nm bead negative control sample. This is caused by the difference in the relative orientation of the single domain nanoparticle magnetic moments inside the beads for the differently sized bead batches. The vector sum of the single domain nanoparticle magnetic moments per bead is larger for 80 nm beads than for 40 nm beads for which the nanoparticle moments are more randomly oriented relative to each other. Another observation is that the decrease of the HFP level due to bead immobilization is different for the differently sized bead batches. The 300 pM m'' curves for the 130 and 250 nm bead samples are close to zero for the entire frequency interval under study, which is not the case for the corresponding 40 and 80 nm bead sample curves.

Effect of Oligonucleotide Surface Coverage. One explanation for this is that the different bead batches have differing oligonucleotide surface coverage (see Table 1). In previous work, it has been observed that the bead immobilization efficiency increases with increasing oligonucleotide surface coverage and that the oligonucleotide coupling yield increases with increasing bead size for the SPDP coupling chemistry.[15] An explanation for the latter could be that larger beads have more amino groups per unit surface area (see Table 1).

Effect of Bead Concentration. A second explanation for the higher bead immobilization efficiency observed for larger beads in Figure 1a is related to the difference in bead concentration. For the 300 pM samples, the ratio between the total number of beads and RCA coils decreases with increasing bead size. For the 40 and 250 nm beads, the ratio between the total number of beads and RCA coils is 49 and 0.18, respectively;[15] the larger number of 40 nm beads is required because of the relatively weaker magnetic moment of these beads.

Effect of Bead Size. In Figure 1b, LFPs are clearly visible at a few hertz for all 300 pM samples except for the sample with 250 nm beads. The observed difference in height of this peak may indicate that the bead size affects whether the beads bind to the exterior or the interior of the RCA coils where the 250 nm beads probably immobilize to mainly give clusters of beads and RCA coils (f_B values much less than 1 Hz at 37 °C), i.e., linking RCA coils together, whereas for smaller bead sizes isolated RCA coils with beads inside coils most likely are formed to a large extent. In fact, it has been shown previously[14,15] that when 40 nm beads (3 and 14 oligonucleotides per bead) were used, clear and narrow LFPs appeared for each RCA coil concentration and both turn-on and turn-off detection were possible. For 130 nm beads (18 oligonucleotides per bead), the LFPs were broad and low in magnitude and there was no correlation between the LFP levels and RCA coil concentrations; only turn-off detection was practically possible. When 250 nm beads (54 oligonucleotides per bead) were used, no LFPs were visible and only turn-off detection was possible. Just like the observations made by analyzing Figure 1b, this suggests that 40 nm beads more easily diffuse into—and hybridize in—the interior sites of the coils due to their small size, thereby forming isolated RCA coils containing immobilized beads, having a relaxation frequency of a few hertz at 37 °C. It further suggests that the 130 nm beads can partly do this but they probably also

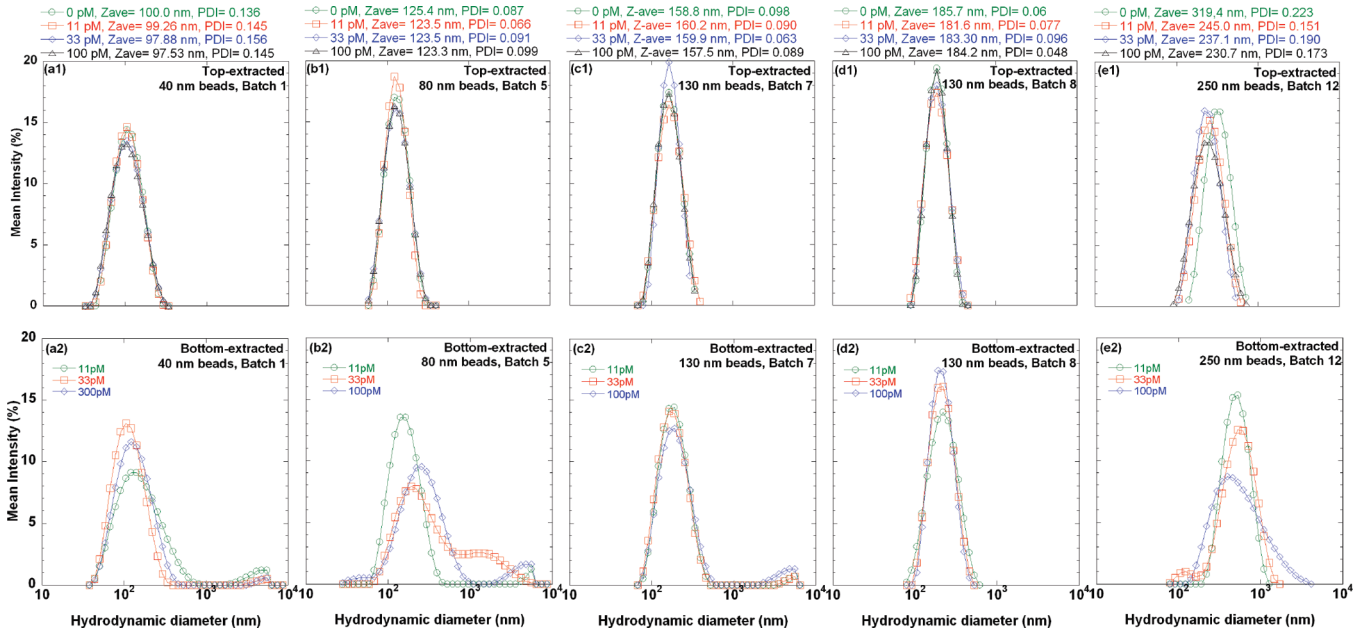

Figure 2. Hydrodynamic size distributions obtained from DLS characterizations of top-extracted and bottom-extracted samples containing the displayed bead types and different RCA coil concentrations. *Z*-average and PDI values are indicated for each of the top-extracted samples. Lines are guides for the eye.

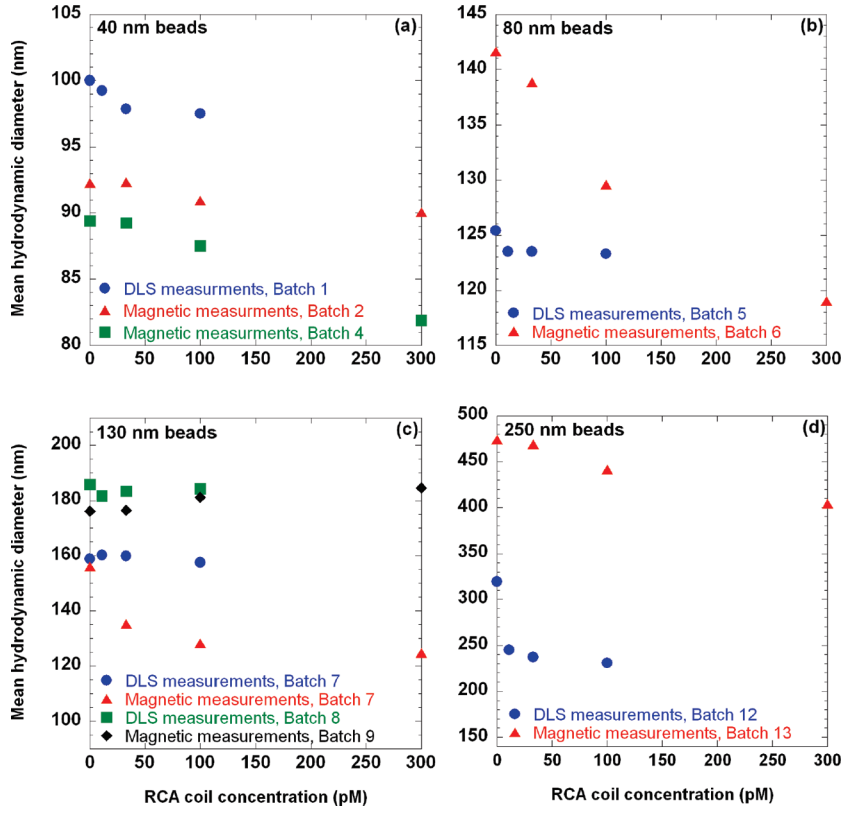

Figure 3. Mean hydrodynamic diameter vs RCA coil concentration for the non-immobilized bead population obtained from complex magnetization measurements (HFPs) and DLS measurements (top-extracted samples). Batches used are indicated in the figure panels.

hybridize to the exterior sites of the RCA coils, thereby linking several coils together to clusters with a broad size distribution. Finally, 250 nm beads most likely mainly hybridize to the exterior of the coils. These assumptions regarding the immobilization behavior are supported by the DLS results presented in the lower panels of Figure 2, presented and discussed below.

3.2. Non-immobilized Beads Studied by Magnetic Measurements and DLS. Figure 2 shows DLS spectra for both top-extracted (panels a1−e1) and bottom-extracted (panels a2−e2) samples containing the differently sized beads under study and selected RCA coil concentrations. We first analyze the behavior of the beads that have not hybridized to the RCA coils, i.e., the beads in the top-extracted samples of Figure 2 as well as those giving rise to the HFP in Figure 1a: Figure 3 shows the mean hydrodynamic diameter vs RCA coil concentration for the non-immobilized bead population obtained from complex magnetization measurements (mean hydrodynamic diameter calculated

from Equation S2 in the Supporting Information using f_B values for the HFPs in Figure S1 in the Supporting Information obtained from Cole−Cole fits) and DLS measurements (top-extracted samples, mean hydrodynamic diameter equal to the *Z*-average values obtained from the upper panels of Figure 2).

Effect of Oligonucleotide Surface Coverage. The mean hydrodynamic diameter tends to decrease for all bead samples, except for batches 8 and 9 (130 nm), with increasing RCA coil concentration. This indicates that large beads in the size distribution are preferentially immobilized. Herein the term "size distribution" is used to describe the distribution in sizes of non-immobilized beads in one particular bead batch. A possible explanation for this observation is that large beads in the size distribution have a larger oligonucleotide surface coverage and therefore immobilize easier than the smaller beads in the same distribution.

Effect of Bead Polydispersity Index. It is also observed that the bead batches with the broadest size distribution (highest PDI, cf. Table 1), viz., the 250 and 40 nm bead batches under study, display the largest decrease in DLS hydrodynamic diameter with increasing coil concentration. The 130 nm bead sample of batches 8 and 9 (Figure 3, panel c), behaves differently: the size distribution is more or less unaffected by the immobilization with an almost insignificant tendency for the smaller beads in the size distribution to preferentially immobilize. The explanation for this is most likely related to the very narrow size distribution of these beads (low PDI, cf. Table 1). It can be observed that the mean hydrodynamic bead sizes for the 0 pM samples is considerably larger than the nominal sizes of the non-functionalized beads. This is caused by the presence of a hydration shell surrounding the beads; the bead surface is strongly hydrophilic due to the dextran casing and the attached oligonucleotides. Note also that the 0 pM hydrodynamic sizes vary for the different batches containing beads of the same nominal size. This is most likely caused by a difference in bead concentration and in the oligonucleotide surface coverage of the beads of the different batches.

Normalizing the data in Figure 3 with respect to the mean diameter at zero RCA coil concentration allows for a more detailed study of the relative change in diameter of non-immobilized beads with changing RCA coil concentration. Such normalization (cf. Figure S2 in the Supporting Information) shows that the largest relative change in diameter of non-immobilized beads almost always appears for the magnetic measurements, particularly for the 80 and 130 nm (batch 7) beads. For the 40 (batches 1 and 2) and 130 nm beads (batches 8 and 9), the data points obtained from magnetic and DLS characterization nearly coincide. The mean hydrodynamic diameter for 130 nm batch 8 and 9 beads is almost constant, which is expected since this particular bead batch is nearly monodisperse. Overall, the magnetic and DLS approaches for characterizing preferential immobilization of beads give qualitatively roughly the same conclusions but rather different quantitative results. The last issue might have several explanations. For instance, the two methods involve different kinds of incubation steps and the complex magnetization and DLS spectra are not recorded at the same temperature. Also, the magnetic method analyzes a larger part of the free bead population than the DLS approach due to the particular extraction steps included in the latter method.

3.3. Immobilized Beads Studied by DLS and Fluorescence Microscopy. We next discuss the hydrodynamic size distributions obtained from DLS characterizations of bottom-extracted samples containing the differently sized beads under study and

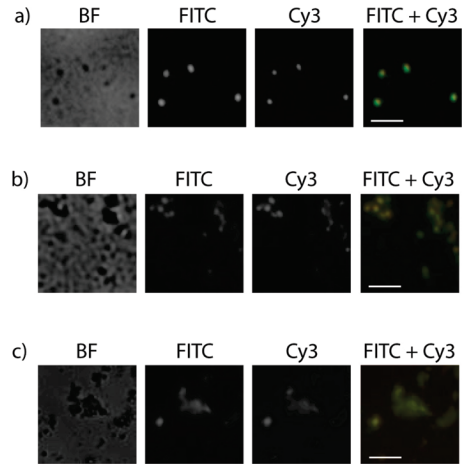

Figure 4. Fluorescence microscopy images of colocalization of RCA coils and oligonucleotide-functionalized magnetic beads (FITC-labeled). The RCA coils were labeled with beads as well as an external detection probe (Cy3-labeled, detection probe 2), and the solution was then deposited on a glass slide and imaged using a fluorescence microscope. (a) Labeling with 40 nm beads (8 oligonucleotides per bead, batch 3 used), results in RCA coils occurring as individual objects. (b) Labeling with 130 nm beads (10 oligonucleotides per bead, batch 10 used), results in clustered RCA coils. (c) Labeling with 130 nm beads (16 oligonucleotides per bead, batch 11 used), results in RCA coils occurring as integrated clusters. The scale bar corresponds to 5 μm.

selected RCA coil concentrations. For both the 40 and 80 nm samples, as well as for the 130 nm sample with the lowest surface coverage of oligonucleotides (batch 7, Figure 2, panel c2), there are two clear peaks for each RCA coil concentration: one small-size peak (SSP) and one large-size peak (LSP). The SSP clearly shows the response from non-immobilized beads, while the LSP most likely originates from isolated RCA coils with immobilized beads and/or smaller clusters of coils. The bottom sediment contains large complexes of RCA coils held together by coil entanglement. The presence of such complexes may explain why the DLS measurements reveal objects being larger than the individual RCA coil size even in the case of the smaller bead sizes.

Effect of Bead Size and Oligonucleotide Surface Coverage. For the 130 nm beads with the highest oligonucleotide surface coverage (batch 8, Figure 2, panel d2) and the 250 nm bead sample, only SSPs are visible for each RCA coil concentration. This indicates that these beads hybridize to a large extent to the exterior of the coils and link several coils together to form clusters of beads and coils falling out of the size window of the DLS instrument. By comparing panels c2 and d2 of Figure 2, it can be concluded that also the oligonucleotide surface coverage affects the immobilization characteristics of the beads. When the beads are too large to easily diffuse to the interior of a coil before hybridization, a high oligonucleotide surface coverage favors the formation of cluster of beads and RCA coils whereas low surface coverage favors the formation of individual RCA coils with beads. The explanation for this is obvious: when a bead is too large to easily diffuse to the interior of a coil before hybridization occurs, the probability of the bead cross-linking several coils increases with the number of oligonucleotides on its surface. Note that only the presence and location of the observed peaks in the DLS spectra in the lower panels of Figure 2 are relevant and not the peak heights since each spectrum is normalized to give peak areas of 100%.

Figure 4 shows representative fluorescence microscopy images of samples with RCA coils and beads (batches 3, 10, and 11, corresponding to 40, 130, and 130 nm beads, respectively,

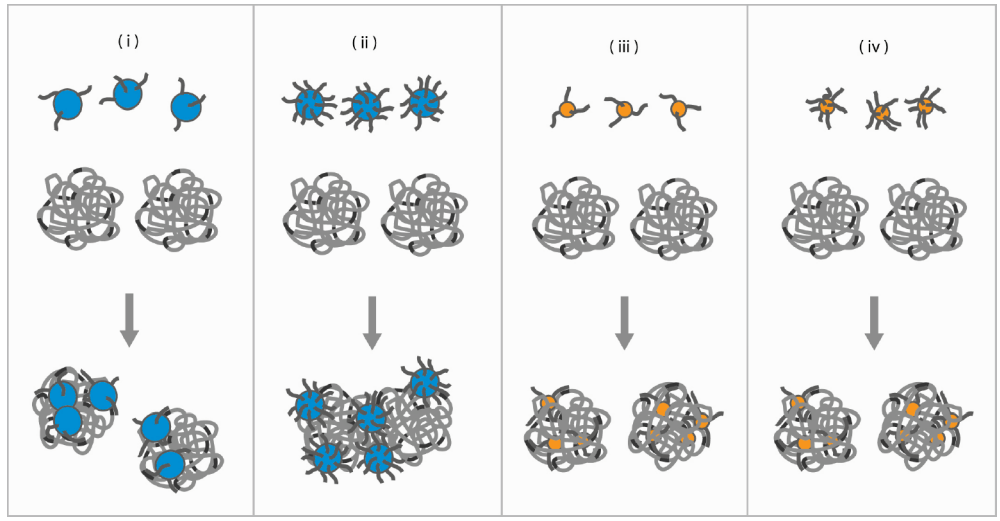

Figure 5. Illustration of the immobilization characteristics of oligonucleotide-functionalized magnetic beads. Larger beads with low oligonucleotide surface coverage (i) form isolated RCA coil containing beads. Larger beads with high oligonucleotide surface coverage (ii) do not form isolated RCA coil containing beads; they link several coils together. Smaller beads with low (iii) and high (iv) oligonucleotide surface coverage form isolated RCA coil containing beads.

were used in panels a, b and c, respectively). Cy3-labeled oligonucleotides were hybridized at another position other than the bead oligonucleotides (FITC-labeled) so that co-localization of beads and RCA coils could be studied. It can be observed that 40 nm beads (batch 3) with a surface coverage of eight oligonucleotides immobilize to give individual RCA coils with beads trapped inside coils (Figure 4, panel a), while 130 nm beads with 10 oligonucleotides immobilize to give clusters of beads and RCA coils (Figure 4, panel b). Moreover, the results for 130 nm beads with 16 oligonucleotides indicate a slightly larger size for coil clusters (Figure 4, panel c). Thus, these measurements confirm the above presented results obtained from the magnetic measurements and DLS analyses that both bead size and oligonucleotide surface coverage influence whether beads immobilize to give isolated RCA coils with beads trapped inside coils or clusters of beads and RCA coils. Figure 5 provides a schematic illustration of the bead-in-a-coil structure for different bead sizes and differing oligonucleotide surface coverage. It shows that for small beads, irrespective of oligonucleotide surface coverage, as well as for large beads with low oligonucleotide surface coverage isolated RCA coils with beads exist (Figure 5, panels i, iii, and iv). For large beads with high oligonucleotide surface coverage, on the other hand, the beads link several coils together to clusters and isolated RCA coils with beads cannot be detected (Figure 5, panel ii).

It would be highly advantageous to be able to image the DNA coil structure containing the immobilized beads using transmission electron microscopy in order to have statistical data from images to support the conclusion put forward in the present paper based on magnetic measurements, DLS, and fluorescence spectroscopy. A method to do this is presently under development.

4. Summary and Conclusions

In this paper we have in detail evaluated the bead immobilization characteristics for the VAM-NDA bioassay, i.e., how oligonucleotide-functionalized magnetic beads with nominal sizes of 40, 80, 130, and 250 nm immobilize to RCA coils. Three experimental methodologies were applied: complex magnetization measurements, DLS and fluorescence microscopy. Overall, it was found that the results obtained from these three characterization techniques were consistent with each other. The most important conclusions concerning bead immobilization characteristics are the following: (i) For beads with a polydisperse particle size distribution, larger beads in the size distribution preferentially immobilize. This is possibly related to a higher oligonucleotide surface coverage for such beads. (ii) Both bead size and oligonucleotide surface coverage determine whether beads immobilize to give isolated RCA coils with beads inside coils or larger clusters of beads and RCA coils. A small bead size and a low oligonucleotide surface coverage favor the first kind of immobilization behavior, whereas a large bead size and high oligonucleotide surface coverage favor the other.

The present findings could be used to optimize both size and surface functionalization of beads employed in substrate-free magnetic biosensors.

Acknowledgment. The Knut and Alice Wallenberg Foundation (KAW), the Swedish Foundation for Strategic Research (SSF), the Swedish Defense Nanotechnology program, and the Swedish Research Council (VR) are gratefully acknowledged for their financial support.

Supporting Information Available: Figures S1 and S2 as well as background information to magnetic characterization and DLS. This material is available free of charge via the Internet at http://pubs.acs.org.

References and Notes

(1) Sassolas, A.; Leca-Bouvier, B. D.; Blum, L. J. *Chem. Rev.* **2008**, *108*, 109.
(2) Flynn, E. R.; Bryant, H. C. *Phys. Med. Biol.* **2005**, *50*, 1273.
(3) Erickson, D.; Mandal, S.; Yang, A. H. J.; Cordovez, B. *Microfluidics Nanofluidics* **2008**, *4*, 33.
(4) Salata, O. V. *J. Nanobiotechnol.* **2004**, 2:3.
(5) Roy, I.; Ohulchanskyy, T. Y.; Pudavar, H. E.; Bergey, E. J.; Oseroff, A. R.; Morgan, J.; Dougherty, T. J.; Prasad, P. N. *J. Am. Chem. Soc.* **2003**, *125*, 7860.
(6) Mornet, S.; Vasseur, S.; Grasset, F.; Duguet, E. *J. Mater. Chem.* **2004**, *14*, 2161.
(7) Svedlindh, P.; Gunnarsson, K.; Strömberg, M.; Oscarsson, S. *Bionanomagnetism in Nanomagnetism and Spintronics—Fabrication, Materials, Characterization and Applications*; World Scientific Publishing: River Edge, NJ, 2009.

(8) Lee, W.; Joo, S.; Kim, S. U.; Rhie, K.; Hong, J.; Shin, K. H.; Kim, K. H. *Appl. Phys. Lett.* **2009**, *94*, 153903.

(9) Sandhu, A.; Sanbonsugi, H.; Shibasaki, I.; Abe, M.; Handa, H. *Jpn. J. Appl. Phys., Part 2: Lett. Express Lett.* **2004**, *43*, L868.

(10) Schotter, J.; Kamp, P. B.; Becker, A.; Puhler, A.; Reiss, G.; Bruckl, H. *Biosens. Bioelectron.* **2004**, *19*, 1149.

(11) Schotter, J.; Panhorst, M.; Brzeska, M.; Kamp, P. B.; Becker, A.; Puhler, A.; Reiss, G.; Brueckl, H. *Molecular detection with magnetic labels and magnetoresistive sensors in Nanoscale Devices—Fundamentals and Applications*; Springer: Dordrecht, Netherlands, 2006; Vol. 233.

(12) Connolly, J.; St Pierre, T. G. *J. Magn. Magn. Mater.* **2001**, *225*, 156.

(13) Astalan, A. P.; Ahrentorp, F.; Johansson, C.; Larsson, K.; Krozer, A. *Biosens. Bioelectron.* **2004**, *19*, 945.

(14) Strömberg, M.; Göransson, J.; Gunnarsson, K.; Nilsson, M.; Svedlindh, P.; Strømme, M. *Nano Lett.* **2008**, *8*, 816.

(15) Strömberg, M.; Zardán Gómez de la Torre, T.; Göransson, J.; Gunnarsson, K.; Nilsson, M.; Strømme, M.; Svedlindh, P. *Biosens. Bioelectron.* **2008**, *24*, 696.

(16) Strömberg, M.; Zardán Gómez de la Torre, T.; Göransson, J.; Gunnarsson, K.; Nilsson, M.; Svedlindh, P.; Strømme, M. *Anal. Chem.* **2009**, *81*, 3398.

(17) Nilsson, M.; Malmgren, H.; Samiotaki, M.; Kwiatkowski, M.; Chowdhary, B. P.; Landegren, U. *Science* **1994**, *265*, 2085.

(18) Landegren, U.; Dahl, F.; Nilsson, M.; Fredriksson, S.; Baner, J.; Gullberg, M.; Jarvius, J.; Gustafsdottir, S.; Soderberg, O.; Ericsson, O.; Stenberg, J.; Schallmeiner, E. *Comp. Funct. Genomics* **2003**, *4*, 525.

(19) Fire, A.; Xu, S. Q. *Proc. Natl. Acad. Sci. U.S.A.* **1995**, *92*, 4641.

(20) Baner, J.; Nilsson, M.; Mendel-Hartvig, M.; Landegren, U. *Nucleic Acids Res.* **1998**, *26*, 5073.

(21) Strömberg, M.; Gunnarsson, K.; Johansson, H.; Nilsson, M.; Svedlindh, P.; Strømme, M. *J. Phys. D: Appl. Phys.* **2007**, *40*, 1320.

(22) Strömberg, M.; Gunnarsson, K.; Valizadeh, S.; Svedlindh, P.; Strømme, M. *J. Appl. Phys.* **2007**, *101*, 023911.

JP911251K